Egypt. J. Chem. **Vol. 67** No. 3 pp. 181 - 193 (2024)

Egyptian Journal of Chemistry

http://ejchem.journals.ekb.eg/

Preparation and Characterization of Graphene Oxide from Agriculture Waste for Water Treatment

Mustafa H. Hafez [a,*], Gehad G. Mohamed [a,b], Mohamed M. Omar [a], Maher M.I. El-Dessouky [a], Tarek S. Jamil [c]

[a] *Chemistry Department, Faculty of Science, Cairo University, 1 Gamaa Street, Giza, P.O. Box 12613, Egypt*

[b] *Department of Nanoscience, Basic and Applied Science Institute, Egypt-Japan University of Science and Technology, New Borg El Arab, Alexandria, 21934, Egypt*

[c] *Water Pollution Research Department, National Research Center, El Behouth Street, Dokki, Giza, P.O. Box 12622, Egypt.*

Abstract

Polycyclic aromatic hydrocarbons (PAHs) like naphthalene (NAPH) are environmentally concerning, impacting aquatic life and human health, NAPH often originates from industries like plastics, fuels, and dyes. This study presents a cost-effective method using rice husk (RH)-derived graphene oxide (GO) to efficiently remove NAPH from water, alongside graphite (G) synthesis for comparison. The prepared GO and G were fully characterized via FT-IR, XRD, TEM, and BET, showing GO's higher BET surface area. Their NAPH adsorption capacities were studied under various conditions, revealing GO's superiority (256.0 µg/g) over G (141.4 µg/g) at pH 5, contact time of 60 min, T = 25 °C and doses of 0.75 g/L (GO) and 1.25 g/L (G). Experimental data for GO and G were analyzed using kinetic and isotherm models, indicating a preference for Pseudo-second order and Langmuir isotherm for NAPH adsorption. In conclusion, the findings underscore the efficacy of RH-based GO as a robust adsorbent for NAPH removal from water, presenting a sustainable and cost-effective avenue for producing GO and its promising application in water treatment.

Keywords**:** Rice husk (RH); Graphene oxide (GO); Graphite (G); Polycyclic Aromatic Hydrocarbons (PAHs); Naphthalene (NAPH); Adsorption; Isothermal; kinetics.

1. Introduction

PAHs, known as polycyclic aromatic hydrocarbons which are organic compounds, are present in large amounts in the environment, including water, air, and soil, and that result from partial fossil fuel combustion, biomass, and other organic materials [1, 2]. There are 16 polycyclic aromatic hydrocarbons that the US Environmental Protection Agency (USEPA) has categorized as important pollutants, one of the most frequent PAHs is naphthalene (NAPH)[3]. It is commonly used in a variety of industrial and household products that include widely utilized in the manufacturing of plastics, dyes, and solvents, also a result of burning fossil fuels, it may be found in crude oil and coal tar. but it is also a frequent environmental pollutant found in water, soil, and air [2, 4-6].

Water pollution is an important environmental issue caused by the release of various chemicals and contaminants into water. PAHs, especially NAPH, contribute significantly to water pollution and are hazardous to both human health and marine life. In aquatic life, it is harmful to fish and other aquatic species and can cause a wide range of health issues, including death. Furthermore, by lowering the quantity of aquatic species at the bottom of the food chain, NAPH could affect the food chain. In human health, it can cause headaches, nausea, and

*Corresponding author e-mail: mustafahafez@gstd.sci.cu.edu.eg; (Mustafa H. Hafez).
Receive Date: 03 August 2023 Revise Date: 27 August 2023 Accept Date: 29 August 2023
DOI: 10.21608/EJCHEM.2023.227014.8359

respiratory issues when swallowed or inhaled. Long-term NAPH exposure can potentially raise the risk of cancer. Furthermore, NAPH can contaminate groundwater by accumulating in sediments and soil over time and contaminate drinking water, causing a variety of diseases, particularly in individuals like children and pregnant women [7-10]. So, individuals and industries must take action to prevent NAPH contamination and appropriately dispose of NAPH-containing products in order to protect our water supplies. Thus, Multiple methods such as catalytic degradation, photocatalytic degradation, and biodegradation have been used to remove NAPH from industrial wastewater and aquatic systems. These techniques' use has several limitations, such as most contaminants are not very biodegradable. Additionally, when pollutants degrade, a few known and unknown metabolites are produced, some of which may be more harmful than the original chemical [11-14]. One of the potent, high-performance, diverse, and easy-to-use techniques is adsorption. It is a technique that removes contaminants from a fluid by attracting them to the surface of adsorbent material [15, 16].

Agricultural waste, such as rice husk (RH), is a significant environmental hazard due to its vast volume and slow decomposition rate. However, recent research indicates that RH may be turned into useful materials such as graphite (G) and graphene oxide (GO), which have the potential for a variety of environmental applications such as the adsorption of contaminants from water [17-20]. GO has special characteristics that make it excellent for environmental applications, such as large surface area, excellent adsorption capacity, and chemical stability. G may be obtained from RH through a technique known as pyrolysis to form a carbon-rich substance. This material may then be treated further to make GO, which has a higher adsorption capacity due to its highly porous and layered structure [21-23]. Multiple environmental and health advantages result from the conversion of RH into G and GO for use in water treatment. Firstly, it reduces the environmental effect of agricultural waste by finding a useful use for it instead of simply throwing it in landfills. Secondly, the utilization of GO for the removal of contaminants from water can enhance water quality for both human and environmental health by minimizing the risk of exposure to dangerous chemicals like NAPH [24-26].

In this paper, we prepare G and GO from RH, as well as study the adsorption of NAPH from water using G and GO. It has been investigated how NAPH adsorption is impacted by contact time, G and GO dosage, and pH. NAPH 's adsorption on G and GO was further assessed using Langmuir and Freundlich isotherms. in addition to Dubinin–Kaganer–Raduskevich (DKR) model, Temkin, and Kinetics studies. G and GO can be recycled for NAPH removal. Furthermore, recycled NAPH can be utilized for further commercial purposes. So, this study could contribute to mitigating the impact of agricultural waste on the environment and human health. Additionally, the use of GO could contribute to industrial wastewater treatment by removing NAPH.

2. Materials and Methods

2.1. Materials

2.1.1. Collection and preparation of samples

RH collected from Fayoum City in Egypt, underwent a process of washing with distilled water to remove any dirt or impurities. Subsequently, it was dried at a temperature of 105 °C for a duration of 90 minutes.

2.1.2. Chemicals and Glasses

GO was synthesized from G derived from RH, while all the chemicals utilized in the experimental procedure were procured from Merck, Germany. The chemicals used included Hydrogen Fluoride (HF), Sodium Nitrate ($NaNO_3$), Sulfuric Acid (H_2SO_4, 98%), Potassium Permanganate ($KMnO_4$), Peroxide Acid (H_2O_2, 30%), Hydrochloric Acid (HCl, 37%), and NaOH from Supelco (Sigma Aldrich, USA). The NAPH standard used in the study was obtained from AccuStandard (USA)1000 µg/mL in MeOH, while Methanol (HPLC grade) was purchased from Sigma Aldrich (USA). The glassware used in the experiment was of grade A from (Normax, Portugal), and Milli-Q water (≥15.1 Ω-cm) was supplied by the Millipore water purification system (Milli-Q).

2.2. Instruments

2.2.1. Instruments for G and GO characterization

The Fourier-transform infrared spectroscopy (FT-IR) to determine functional groups of G and GO was measured using Bruker VERTEX 80 (Germany) combined Platinum Diamond ATR, which includes comprises a diamond disk as that of an internal reflector in the range 4000–400 cm^{-1} with resolution 4 cm^{-1}, refractive index 2.4.

The X-ray diffraction (XRD) measured the crystalline phase of G and GO by Model XPERT-PRO-PANalytical (Netherland) that Anchor Scan Parameters are: Start position 4.0100, end position 79.9900, step size 0.0200, scan step time (S) 0.5000, scan type is continuous, measurement temperature 25 °C, anode material Cu, K-alpha1 (A) 1.54060, K-Alpha2 (A) 1.54443, K-Beta (A) 1.39225, K-A2/K-A1ratio 0.5000, and Generator settings 30mA,45 kV.

The transmission electron microscope (TEM) used for the purpose of imaging, crystal structure revelation, and elemental analysis "qualitative and semi-quantitative analysis by Model Tecnai G20,

Super twin, double tilt (Netherland), Applied voltage: 200 KV, Magnification Range: up to 1,000,000 X, Gun type is LaB_6 Gun, two imaging modes were employed, namely bright field imaging using a LaB_6 electron source gun with an electron accelerating voltage of 200 KV, and diffraction pattern imaging. A CCD camera with a resolution of 4k*4k was used to acquire and collect transmitted electron images. To acquire and analyze EDX peaks, TEM Imaging & Analysis (TIA) software was utilized for spectrum acquisition and analysis.

The specific surface area and total pore volume were investigated using the Brunauer-Emmett-Teller (BET) method using a high-throughput surface area and pore size analyzer (BELSORP MAX, Japan) [27].

2.2.2. Instruments for experimental work

Purge Gas Chromatography-Mass spectrometry (Purge GC-MS) is used for measuring the concentration of NAPH in aqueous solution by Purge Model OI Analytical Eclipse 4660, and GS-MS Model 7890AGC system, 5975C inert MSD with triple axis detector (Agilent, USA) with Flow 1 for 8 minutes, then increase with rate 0.5 to Flow 2. The type of column is DB-VRX with a length of 60 meters, inner diameter of 250 µm, and film thickness of 1.4 µm.

The solution's pH was measured by using the pH Jenco 6173 Model (USA) and corrected using 1 mol/L H_2SO_4 or NaOH.

Digital Orbital Shaker used for shaking the aqueous solution with 120 rpm by Model SHO-2D, (Korea). Digital analytical balance ADAM, Model PW214, (England).

2.3. Methods

2.3.1. G Preparation

RH was dried in a dry oven where it was filtered and ground. then put in a furnace and burned for three hours at 550 °C at atmospheric pressure. It is very silica-rich. As a result, HF was used to eliminate silica. 30 mL of 40% HF was used to dissolve 10 g of G, which was then heated and stirred for three hours. The suspension was then dried after being cleaned with distilled water [28].

2.3.2. GO Preparation

By using the modified Hummers method as shown in Figure 1, 5g of prepared G was added carefully to 2.5 g of $NaNO_3$ and 115 mL of H_2SO_4 (98%) in an ice bath to prevent raising in the temperature, with stirring for 2 hours, then gradually add 15 g of $KMnO_4$ with stirring for 2 hours. Once the ice bath was eliminated, the reaction mixture was stirred for 30 minutes while being covered with aluminum foil, resulting in the formation of a brown paste. Subsequently, the reaction mixture was carefully diluted with 230 mL of DI water, ensuring that the temperature remained below 100 °C. While stirring the mixture for an hour, 700 mL of DI water was added to dilute it. Following that, 10 mL of 30% H_2O_2 was introduced, causing the mixture to transform into a yellow color. The resulting mixture underwent centrifugation and was washed multiple times using a 5% HCl aqueous solution and DI water. Lastly, the resulting solid was dried at 60 °C for 24 hours, resulting in a loose brown powder [23, 29].

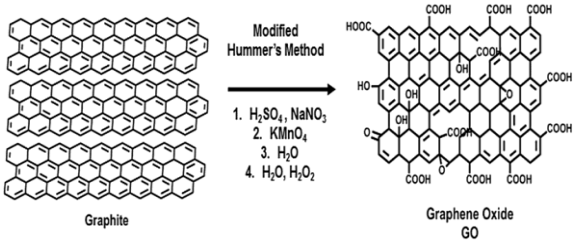

Figure 1. Preparation of GO from G by modified Hummer's methods [30].

2.3.3. Preparation of NAPH solution

The chemical formula for NAPH is $C_{10}H_8$, Molecular weight is 128.2 and CAS.NO is 91-20-3. It is a white, crystalline solid, that slowly dissolves at room temperature and has a characteristic odor with a melting point of 80.5 °C and a boiling point of 218 °C, and its solubility in water is 31.7 mg/L. The partial pressure of its vapor is 0.087 mmHg at 25 °C, and Log K_{ow} "K_{ow}: octanol–water partition coefficient" is 3.33. The toxic Equivalent Factor (TEF) is 0.001. The Chemical Structure of NAPH is shown in Figure 2 [1, 9, 31].

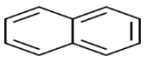

Figure 2. Structure of naphthalene (NAPH).

NAPH stock standard concentration of 200 µg/mL was prepared in methanol by NAPH standard solution 1000 µg/mL then NAPH aqueous solution of 200 µg/L was prepared in fresh Milli-Q water. Calibration of NAPH with concentration levels of 5, 10, 20, 30, and 50 µg/L were prepared in fresh Milli-Q water. Samples and the NAPH stock standard were kept in sealed glass and kept at 4 °C in the refrigerator.

2.3.4. Adsorption studies

At room temperature, the adsorption of NAPH from aqueous solutions on adsorbents was studied. Several tests were conducted using 500 mg/L of adsorbent and 200 µg/L of adsorbate in order to investigate the effects of time, pH, and adsorbent dosage on the adsorption processes. 50 mg of adsorbent and 0.1 L of NAPH aqueous solution are added to each of 100 mL closed conical flasks. Every

ten minutes during 60, (120, and 180 minutes), the covered conical flasks were shaken on a Digital Shaker at 120 rpm at a constant temperature 25 °C. Double Rings 102 filter paper was used to filter the sample. A Purge GC-MS was used to quantify the initial and equilibrium concentrations of the aqueous solutions. The removal efficiency (R%) was calculated by using Eq.1, and the quantity of adsorption (q_e µg/g) by using Eq. 2:

$$R\% = \frac{C_\circ - C_e}{C_\circ} \times 100 \quad (1)$$

$$q_e = \frac{C_\circ - C_e}{w} \times v \quad (2)$$

Where C_o indicates to the initial concentration of adsorbate (µg/L), C_e indicates the concentration of adsorbate solution (µg/L) at time t, v corresponds to the volume of the solution (L), and w indicates the weight of adsorbent (g) [32].

The effect of the adsorbent dose was investigated using adsorbent weights of 0.025, 0.05, 0.1, 0.125, and 0.15 g in 100 mL of 200 µg/L of NAPH, while the effect of pH was examined using pH values of 3, 5, 7, 9, and 11; the pH was modified using 1 mol/L H_2SO_4 or NaOH.

2.3.5. Adsorption Isothermal

The Langmuir and Freundlich isothermal models of adsorption were suited using various concentrations of adsorbate at room temperature. In the Langmuir isothermal model, NAPH adsorption occurs as a monolayer on the adsorbent's outer surface [33, 34], as shown by the expression:

$$q_e = \frac{q_{max} * bC_e}{1 + bC_e} \quad (3)$$

Eq. 3's linearized version is as follows:

$$\frac{c_e}{q_e} = \frac{1}{q_{\max} * b} + \left(\frac{1}{q_{\max}}\right) c_e \quad (4)$$

Where c_e is the NAPH equilibrium concentration in solution (µg/L), q_e is the quantity of NAPH sorbed per unit mass of adsorbents (µg/g), and $q_{\max}$and b are the Langmuir constants for monolayer sorption capacity (µg/g) and the equilibrium constant of Langmuir (L/µg), respectively. By $C_\circ$ initial concentration of NAPH in solution and calculated Langmuir constant equilibrium (b), we get the constant dimensionless separation factor R_L as following Eq.:

$$R_L = \frac{1}{1 + bC_\circ} \quad (5)$$

According to R_L, the form and favorability of the adsorption between adsorbents and NAPH may be explained. The value of R_L shows whether the isotherm has an unfavorable (R_L>1), a linear shape (R_L = 1), a favorable (0 <R_L<1), or an irreversible (R_L = 0) [35].

The Freundlich model indicates that NAPH adsorption occurs in multilayer and heterogeneous adsorption. The model's expression can be shown as :

$$q_e = K_f C_e^{1/n} \quad (6)$$

The following constants and logarithms can be used to make this expression linear:

$$log\, q_e = log k_f + \frac{1}{n} log\, C_e \quad (7)$$

Where $\frac{1}{n}$ is the adsorption intensity, which is correlated with the heterogeneity of the adsorbent surface, and K_f is the adsorption capacity (L/µg) for the adsorbent [36].

Dubinin–Kaganer–Raduskevich (DKR) isotherm is used to determine the apparent energy of NAPH adsorption onto adsorbent and has the following linear form [37, 38]:

$$ln\, q_e = ln\, q_{max} - \beta\varepsilon^2 \quad (8)$$

$$\varepsilon = RT\, ln\left(1 + \frac{1}{c_e}\right) \quad (9)$$

Where q_{max} stands for maximal sorption capacity (µg/g), β for an activity coefficient constant relating to sorption energy, and ε for Polanyi potential. the mean free energy (E) of sorption per sorbate molecule transported to the solid's surface from infinity in the solution as following Eq. [32, 39]:

$$E = \frac{1}{\sqrt{2\beta}} \quad (10)$$

If E is between 8 and 16 kJ mol^{-1}, the adsorption process is mostly based on an ion exchange mechanism. If E is less than 8.0 kJ mol^{-1}, physical interactions can explain the adsorption. Adsorption can be explained by chemical interactions if E is more than 16 kJ mol^{-1}[32].

The Temkin isotherm is commonly used to non-uniform sorption heat distribution [40].

$$q_e = \frac{RT}{b} ln\, A + \frac{RT}{b} ln\, C_e \quad (11)$$

The equilibrium binding constant, A (L /mol), represents the highest possible binding energy. B is the adsorption's heat constant. where: B= $\frac{RT}{b}$ constant correlated to the heat of sorption (J/mol) derived from

the Temkin plot (q_e versus ln C_e); R= universal gas constant (8.314 $J.mol^{-1}.K^{-1}$) T= Temperature (25 °C= 298 K) [41].

2.3.6. Adsorption kinetics

To accommodate the experimental data, several kinetic models were used, including the Pseudo-first order model, the Pseudo-second order model, and the Intra-particle diffusion model. Adsorption kinetics equations are as following:

$$log(q_e - q_t) = log\, q_e - \left(\frac{k_1}{2 \cdot 303}\right) t \quad (12)$$

$$\frac{t}{q_t} = \left(\frac{1}{k_2 q_e^2}\right) + \left(\frac{1}{q_e}\right) t \quad (13)$$

$$q_t = k_i t^{0.5} + C \quad (14)$$

Where Eq.12, Eq.13, and Eq.14 are the Pseudo-first order model, the Pseudo-second order model, and the Intra-particle diffusion model, respectively. q_t and q_e the quantities of NAPH adsorbed (µg/g) at time t and equilibrium, respectively. k_1 (min^{-1}) and k_2 ($g.µg^{-1}.min^{-1}$) are the adsorption rate constants of the Pseudo-first order and Pseudo-second order expressions, respectively, k_i is the Intra-particle diffusion rate constant (µg. g^{-1}. $min^{1/2}$). C; The boundary layer thickness constant (µg/g) [41, 42].

3. Results and Discussion

3.1. Characterization of adsorbents

3.1.1. FT-IR spectroscopy analysis

FT-IR analysis helps us understand the chemical bonds and functional groups in G and GO and how they affect the adsorption of NAPH. As seen in Figure 3 depicts the FT-IR of G, It is a two-dimensional (2D) structure made up of parallel layers of hexagonal rings of carbon atoms sp^2 hybridized. There are no prominent peaks in the FT-IR spectra of G that are relevant to any functional groups, but weak bands may occur [43, 44]. But in FT-IR spectrum of GO, because of the existence of oxygen functional groups, GO often exhibits numerous absorption bands as compared to G. a broad absorption band at 3277 cm^{-1}, corresponding to hydroxyl and carboxyl group stretching vibrations, as well as a significant absorption band about 1721 cm^{-1}, which corresponds to the stretching vibration of carbonyl groups, are the most notable bands in GO. The C-O may be seen in the band at 1418 cm^{-1}, 1222 cm^{-1} indicates about the C-O stretching of epoxy groups, and a significant peak from the vibration of water adsorbed on GO superposed with C=C stretching of the graphitic basal plane at 1620 cm^{-1}, the mode at 1031cm^{-1} indicates C-O-C stretching of alkoxy groups [45-47]. FT-IR may also be used to determine the degree of oxidation in GO samples. The intensity of the absorption band at 1721 cm^{-1} is widely used to determine the degree of oxidation. as it rises with increasing oxidation due to additional carbonyl groups present on the GO surface [48].

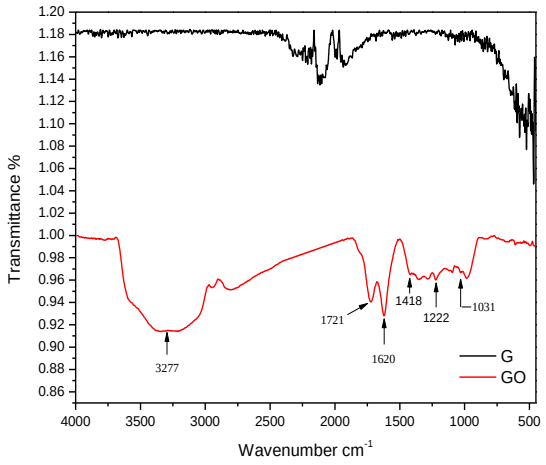

Figure 3. FT-IR spectrum of G and GO.

3.1.2. XRD analysis

XRD is a method that provides specific details on the material's chemical composition and crystalline structure. It is a special instrument that may also be used to find the existence of phases in a substance. to acquire G's structural information, as shown in Figure 4 main peak was noted at [°2θ] = 26.6, similar to the G (002) reflection [49, 50]. while GO's structural information, main a broad peak at [°2θ] = 10.97, similar to the GO (001) reflection, is attributed to the GO surface's oxygen-containing functional groups [51], this referred to G which has been transformed into GO [52].

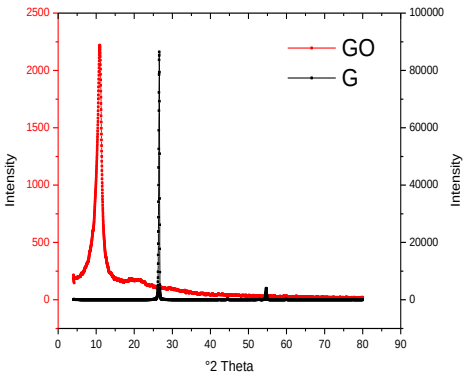

Figure 4. XRD pattern of G and GO.

3.1.3. TEM

As shown in Figure 5, the TEM images of GO revealed a thin, transparent sheet-like structure with a wrinkled or folded appearance. The wrinkles and folds are caused by the GO surface's oxygen

functional groups, which induce mechanical tension and curvature into the graphene lattice [52, 53]. The multilayered structure in GO may indicate pieces that have not been entirely exfoliated or have been restacked together as a result of electrostatic contact, capillary, and Van der Waals forces during the dispersion process [54].

3.1.4. BET analysis

It can offer valuable data on the specific surface area of G and GO and explains gas molecule physical adsorption on a solid surface. the N_2 adsorption-desorption isotherm and pore size distribution of G and GO were calculated and illustrated in Figure 6. Referring to the data presented in Table 1 from the BET analysis, the S_{BET} of G is 9.9769 m^2g^{-1} and the pore size is 57.309 nm, but the S_{BET} of GO is 123.0 m^2g^{-1} and the pore size is 26.866 nm which is much higher than G. G_{BET} analysis often reveals a type II isotherm [55], C = 27.14, where C >1, which is typical of a material with a non-porous surface, which total pore volume ($P/P_{\circ}$=0.951) 0.1429 cm^3g^{-1}. This is due to G's generally flat, smooth surface, which has few flaws or surface imperfections. G typically has a little amount of gas adsorbed on it, and its specific surface area is also small [56]. The S_{BET} of GO, on the other hand, is substantially larger because of its extremely porous structure, which has a total pore volume ($P/P_{\circ}$=0.944) 0.8261 cm^3g^{-1} and contains numerous flaws and surface imperfections [57]. A type IV isotherm, which is indicative of a mesoporous substance with a moderately narrow range of pore sizes, is frequently seen in the BET analysis of GO whose mesopores range from 2-50 nm [55]. In comparison to G, GO has a much higher amount of gas adsorbed on its surface and a larger specific surface area [57].

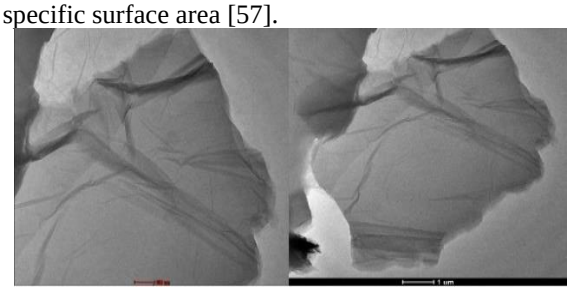

Figure 5. TEM image of GO.

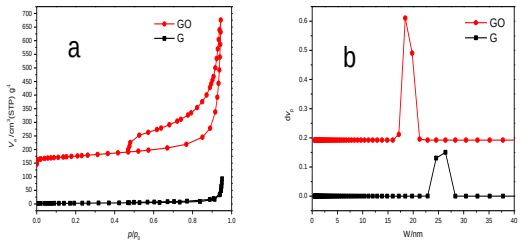

Figure 6. (a) adsorption and desorption isotherm of G and GO (adsorptive N_2, adsorption temp 77[k]), (b) NLDFT/GCMC pore size distribution analysis of G and GO (adsorptive N2, adsorption temp 77[k]).

Table 2. Selected properties of G and GO in BET analysis.

Adsorbent	Surface area S_{BET} m^2g^{-1}	Total Pore volume Cm^3g^{-1}	P/P_o	*Mean pore diameter nm*
G	9.9769	0.1429	0.951	57.309
GO	123.00	0.8261	0.944	26.866

3.2. Effect of contact time

At room temperature (25 ± 0.2 °C), using a mass adsorbent of 0.5 g/L, an initial pH = 5, and an initial NAPH concentration of 200 µg/L, the effect of contact time on G and GO's ability to remove NAPH was investigated. At various contact times for 10-60 min at time intervals of 10 min then 120 min, and 180 min, the removal percentage of NAPH was determined. As shown in Figure 7, NAPH may be adsorbed on G and GO in three stages: the first quick adsorption stage, the slower adsorption stage, and the equilibrium stage. This process is often time-dependent [58]. As in the case of G and GO, the removal rate increases before slowing down until equilibrium is reached after 60 minutes, at which point the removal rate becomes a minor influence until 180 minutes. The decrease in rate over time might be explained by the reduced availability of GO and G active sites. where GO has a higher removal rate than G due to more adsorption sites available on the surface of GO compared to G, resulting in greater accessibility [59].

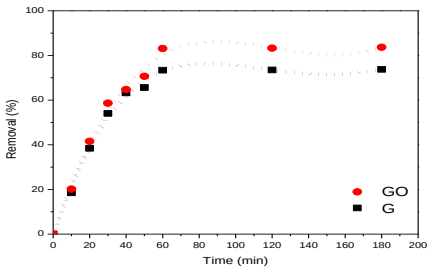

Figure 7. Effect of contact time on the removal of NAPH using G and GO. [NAPH] = 200 µg/L; G and GO dose = 0.5 g/L; T = 25 °C; and pH = 5.

3.3. Effect of the adsorbent dose

At room temperature (25 ± 0.2 °C), several doses of the adsorbent (G and GO) were added to 100 mL of a 200 µg/L solution of NAPH for an optimal shaking time 60 minutes, and pH = 5 to investigate the impact of the adsorbent dose. In Figure 8, the rate of increase in adsorption of NAPH on G and GO increases rapidly at initially but gradually slows. The results show that as the adsorbent dose is increased, NAPH adsorption increases dramatically till 0.075g/100 mL for GO and 0.125 g/mL for G because the GO surface has a greater number of sites for adsorption than the G surface. The dosage of GO and G had no discernible effects above this level. In

the case of GO, as the dosage of GO increased from 0.025 to 0.075 g/100 mL, the removal percentage of NAPH increased from 64.9% to 97.8%. On the other hand, for G, as the dosage increased from 0.025 to 0.125 g/100 mL, the removal percentage of NAPH increased from 53.1% to 89.8% [60]. This is because more absorbent is utilized, resulting in more active sites for adsorbate. However, because the solution contains fewer NAPH molecules, the NAPH molecules are less easily accessible on the adsorbent surface [61].

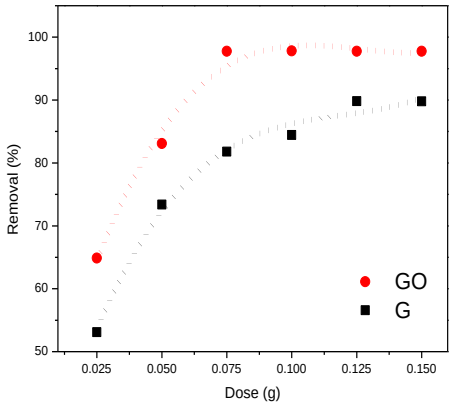

Figure 8. Effect of dose of G and GO on the removal of NAPH. [NAPH]= 200 µg/L; time = 60 min; T = 25 °C and pH = 5.

3.4. Effect of pH

At room temperature (25 ± 0.2 °C), studying the impact of solution pH by using 100 mL of NAPH solution with a concentration of 200 µg/L containing 0.075 g/100 mL of GO and 0.125 g/100 mL of G in the pH range (3, 5, 7, 9, 11). To adjust the pH of the solution, 1 mol/L sulfuric acid and sodium hydroxide were utilized. As shown in Figure 9, the adsorption of NAPH on GO and G was almost independent of solution pH over the investigated pH range because NAPH was non-ionizable. However, its pH 3 adsorbed level was a little high [62].

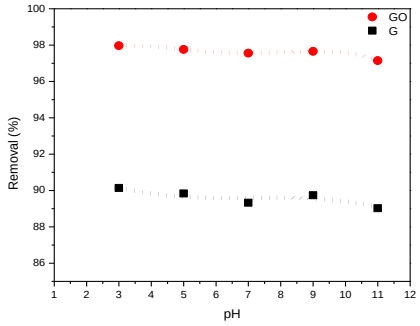

Figure 9. Effect of pH on removal of NAPH using G and GO. [NAPH] = 200 µg/L; time = 60 min; T = 25 °C and G and GO dose = 0.125 and 0.075 g/100 mL, respectively.

3.5. Modeling of adsorption isotherm

For monolayer adsorption at specified homogenous locations on the G and GO surfaces, the Langmuir isotherm is often utilized. As shown in Figure 10, by using Eq. 4 when plotting C_e/q_e against C_e for the Langmuir isotherm, straight lines were obtained. Based on the initial concentration C_o and the Langmuir constant b, use Eq. 5 to calculate the separation factor, R_L, as given in Table 2. The value of R_L denotes the previous equation was positive and less than one, ($0 < R_L < 1$), indicating that NAPH adsorption onto G and GO is favorable [41].

The Freundlich isotherm is widely used in heterogeneous surface energy systems. By Eq. 7, as indicated in Figure 11, the graph that results from plotting log q_e vs log C_e for the Freundlich isotherm has an intercept of K_f and a slope of 1/n. As seen in Table 3, The Freundlich isotherm shows that the 1/n values are between 0 and 1, which indicates that NAPH adsorption onto G and GO is favorable, and the surface of G and GO with NAPH are strongly bound where the values of n in the 1-10 range indicate that NAPH favorable adsorption onto G and GO [63]. The high k_f values show that both G and GO have a strong NAPH adsorption capacity and affinity [29].

As shown in Figure 12, Dubinin–Kaganer–Raduskevich (DKR) Isotherm, by Eq. 8, The DKR parameters are derived from the slope of the plot of ln q_e against ε^2, which yields β (mol^2/J^2), and exp (intercept), as shown in Table 4 which yields q_{max} (µg/g). By Eq. 10, the mean free energy (E) of G and GO are 250 $Jmol^{-1}$, and 845.2 $Jmol^{-1}$, respectively. That is greater than 16 in both cases of G and GO, so it indicates that the sorption process is chemical [32].

As shown in Figure 13, the Temkin isotherm, by Eq. 11, we obtained straight lines while graphing q_e versus ln C_e. Get the Temkin isotherm constant (b) from the line's slope, B=RT/b, and the Temkin isotherm equilibrium binding constant (A), which represents the maximum binding energy, from the line's intercept, RT/b ln A, as indicated in Table 4 [40].

According to the R^2 results, the Langmuir isotherm is more suited for NAPH adsorption on G and GO where correlation coefficient (R^2) are 0.996, and 0.998, respectively. demonstrating that the Langmuir adsorption model accurately simulates the experimental results and demonstrating that the adsorption is monolayer [64, 65]. This implies that the adsorbent's surface, the arrangement of molecules on the surface of the adsorbent, and the nature of the interaction between NAPH and the adsorbent are all variables in the sorption capabilities [61].

Table 3. Values R_L of initial concentrations of NAPH adsorption on (G) and (GO).

C_o µg/L	R_L (G)	R_L(GO)
100	0.17	0.07
150	0.12	0.05
200	0.09	0.04
250	0.08	0.03

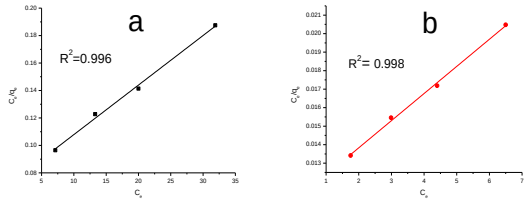

Figure 10. Langmuir isotherm of NAPH adsorption on a- (G) and b- (GO).

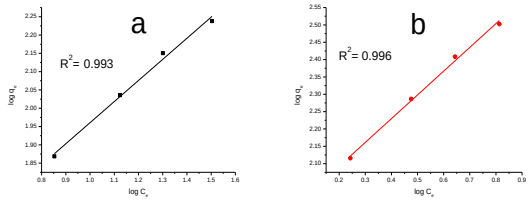

Figure 11. Freundlich isotherm of NAPH adsorption on a- (G) and b- (GO).

Table 4. Langmuir, Freundlich, and R^2 values of NAPH adsorption on G and GO.

Adsorbent	Langmuir Constants			Freundlich Constants			
	q_e	b	R^2	1/n	n	K_f	R^2
G	277.78	0.050	0.996	0.577	1.73	24.2	0.993
GO	666.67	0.138	0.998	0.685	1.46	90.3	0.996

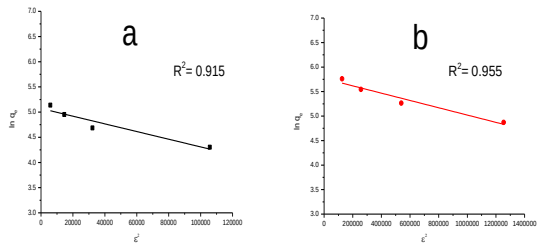

Figure 12. DKR isotherm of NAPH adsorption on a- (G) and b- (GO).

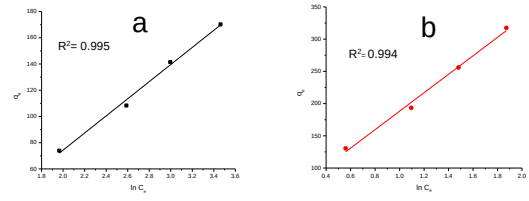

Figure 13. Temkin isotherm of NAPH adsorption on a- (G) and b- (GO).

Table 5: DRK, and Temkin constants and R^2 values of NAPH adsorption on G and GO.

Adsorbent	DKR Constants			Temkin Constants			
	q_{max}	E	R^2	b	A	B	R^2
G	159.35	250.0	0.915	38.0	0.42	65.27	0.995
GO	319.19	845.2	0.955	17.3	1.37	143.3	0.994

3.6. Adsorption kinetics

3.6.1. Pseudo-first order and pseudo-second order

The adsorption kinetics were investigated using the Pseudo-first order and Pseudo-second order kinetic models. As seen in Figure 14 when log (q_e-q_t) vs. time was plotted, A linear relationship was observed for both G and GO when applying the Pseudo-first order model. The R^2 values obtained were 0.820 for G and 0.755 for GO. In contrast, Figure 15 illustrated the R^2 for the straight line resulting in the plot of t/q_t and t for the Pseudo-second Order model for G and GO was 0.878 and 0.891, respectively. as shown in Table 5, Based on the R^2 values, the Pseudo-second order model is more effective and yields higher accuracy compared to the Pseudo-first order model. The calculated adsorption capacity (q_e,cal) derived from the Pseudo-second order model demonstrates better consistency than the experimental adsorption capacity (q_e,exp) [65], also by calculating the square sum of errors (SSE).

$$SSE = \sum \frac{\left(q_{e(\exp.)} - q_{e(cal.)}\right)^2}{q_{e(exp.)}} \quad (15)$$

It can be used to find the perfect fit for kinetics models, the lowest value SSE is the best, it is clear from Eq. 15, Pseudo-second order has a lower SSE than Pseudo-first order [41]. Chemical adsorption was shown to contribute to kinetic data modeling because of the interaction of π electrons of NAPH with the surface of G and GO. These results indicate that the adsorption rate is likely controlled by chemisorption, wherein chemical bonds are formed between the functional groups on the adsorbent's surface and the NAPH molecules. Because of the larger surface area and a greater number of functional groups on the GO surface, NAPH adsorption on GO is often quicker than on G. However, it is important to note that the adsorption kinetics can be influenced by other factors, such as the initial concentration of NAPH in the solution [66].

3.6.2. Intra-particle diffusion

It provides a useful tool to better understand how NAPH is absorbed onto G and GO. According to this model, the rate of adsorption is regulated by the movement of the NAPH within the pores of the adsorbent particles. By Eq. 14 For the Intra-particle diffusion model, Figure 16 When plotting the

relationship between q_t and $t^{0.5}$, it is expected to observe a straight line. However, it is important to note that the line may not pass through the origin, indicating the presence of additional mechanisms involved in the adsorption process [61]. The intra-particle diffusion model applies to NAPH adsorption onto both G and GO, demonstrating that NAPH diffusion within adsorbent particle pores is a significant mechanism in the adsorption process. However, as seen in Table 6 the rate constant k_i for NAPH adsorption onto GO (51.39 µg.g.min$^{0.5}$) is generally greater than that for NAPH adsorption onto G (46.48 µg.g.min$^{0.5}$). The findings suggest that the presence of a larger surface area and increased functional groups on the GO surface leads to faster adsorption of NAPH. However, when the adsorbent particle size decreases, external mass transfer mechanisms become more influential. This can result in a decrease in the overall contribution of Intra-particle diffusion to the adsorption process [49].

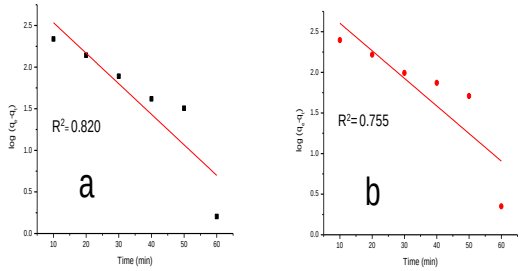

Figure 14. Pseudo-first order of NAPH adsorption on a- (G) and b- (GO).

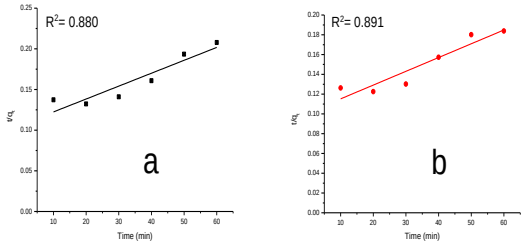

Figure 15. Pseudo-second order of NAPH adsorption on a- (G) and b- (GO).

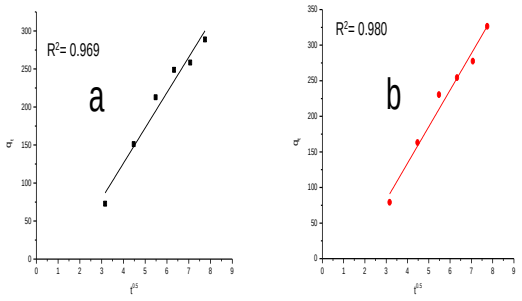

Figure 16. Intra-particle diffusion of NAPH adsorption on a-(G) and b- (GO).

Table 6. Constants and R^2 values of Intra-particle diffusion of G and GO.

Adsorbent	Intra-particle diffusion	
	K_i	R^2
G	46.48	0.969
GO	51.39	0.980

3.7. Desorption and reusability experiments

For eight cycles, the adsorption-desorption studies were performed at room temperature. Using a mixture of methanol and 2%NaOH solution(1:1) [67], NAPH's quantitative desorption was accomplished from G and GO where after filtration and washed with distilled water, can be reused several times. Figure 17 illustrates in the case of GO, more than 90% of the desorption process was effective up to six cycles, but in the case of G, more than 80% up to 5 cycles. The reusability of G and GO shows that the adsorbent is inexpensive and practical and that it may be evaluated and used in wastewater treatment [61].

Table 7. Constants, SSE, and R^2 values of Pseudo-first order and Pseudo-second order of NAPH adsorption on G and GO.

Adsorbent	q_e (exp)	Pseudo-first order				Pseudo-second order			
		q_e (cal)	SSE	K_1	R^2	q_e (cal)	SSE	K_2	R^2
G	141.44	797.99	3048	0.085	0.820	625.00	1653	2.40E-5	0.878
GO	256.00	880.85	1525	7.83E-2	0.755	714.29	820	1.93E-5	0.891

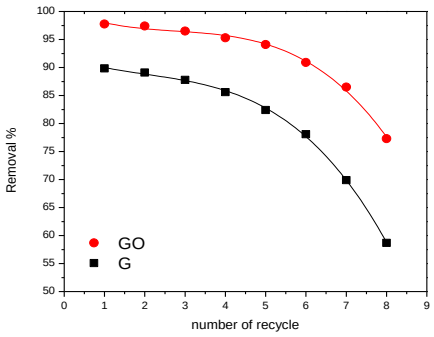

Figure 17. Recycle of G and GO.

4. Conclusion

The conclusion of this study, GO produced from RH has been shown to be an effective material for NAPH adsorption from aqueous solutions. These materials offer various advantages, including low cost, ease of supply, and environmental friendliness, making them viable alternatives to traditional adsorbents. The adsorption process of NAPH on GO is influenced by multiple factors, including contact time, and the amount of GO used. The adsorption of NAPH on GO was not significantly influenced by the pH of the solution. This advantageous quality of GO offers practical benefits, particularly when dealing with wastewater that may have varying pH levels. The adsorption process follows the pseudo-second order kinetics and can be described by the Langmuir isotherm model, indicating the formation of monolayer adsorption on the surface of GO. Overall, the findings suggest that GO has the potential for use in environmental applications as a good adsorbent for removing NAPH from contaminated water.

5. Acknowledgment

This study was supported by CLDWGC and NRC, the authors appreciate the help from everyone who made this effort possible.

6. Reference

[1] I. Abbas, G. Badran, A. Verdin, F. Ledoux, M. Roumié, D. Courcot, *et al.*, "Polycyclic aromatic hydrocarbon derivatives in airborne particulate matter: sources, analysis and toxicity," *Environmental Chemistry Letters*, vol. 16, pp. 439-475, 2018.

[2] A. I. Rubailo and A. V. Oberenko, "Polycyclic aromatic hydrocarbons as priority pollutants," 2008.

[3] A. Mojiri, J. L. Zhou, A. Ohashi, N. Ozaki, and T. Kindaichi, "Comprehensive review of polycyclic aromatic hydrocarbons in water sources, their effects and treatments," *Science of the total environment*, vol. 696, p. 133971, 2019.

[4] S. K. Shukla, N. Mangwani, T. S. Rao, and S. Das, "Biofilm-mediated bioremediation of polycyclic aromatic hydrocarbons," in *Microbial biodegradation and bioremediation*, ed: Elsevier, 2014, pp. 203-232.

[5] S. K. Samanta, O. V. Singh, and R. K. Jain, "Polycyclic aromatic hydrocarbons: environmental pollution and bioremediation," *TRENDS in Biotechnology*, vol. 20, pp. 243-248, 2002.

[6] H. H. Schobert and C. Song, "Chemicals and materials from coal in the 21st century," *Fuel*, vol. 81, pp. 15-32, 2002.

[7] C.-D. Dong, C.-F. Chen, and C.-W. Chen, "Determination of polycyclic aromatic hydrocarbons in industrial harbor sediments by GC-MS," *International journal of environmental research and public health*, vol. 9, pp. 2175-2188, 2012.

[8] M. C. McLaughlin, T. Borch, B. McDevitt, N. R. Warner, and J. Blotevogel, "Water quality assessment downstream of oil and gas produced water discharges intended for beneficial reuse in arid regions," *Science of The Total Environment*, vol. 713, p. 136607, 2020.

[9] R. Preuss, J. Angerer, and H. Drexler, "Naphthalene—an environmental and occupational toxicant," *International archives of occupational and environmental health*, vol. 76, pp. 556-576, 2003.

[10] A. T. Lawal, "Polycyclic aromatic hydrocarbons. A review," *Cogent Environmental Science*, vol. 3, p. 1339841, 2017.

[11] N. Mukwevho, R. Gusain, E. Fosso-Kankeu, N. Kumar, F. Waanders, and S. S. Ray, "Removal of naphthalene from simulated wastewater through adsorption-photodegradation by ZnO/Ag/GO nanocomposite," *Journal of Industrial and Engineering Chemistry*, vol. 81, pp. 393-404, 2020.

[12] C. M. Aguilar, J. L. Rodríguez, I. Chairez, H. Tiznado, and T. Poznyak, "Naphthalene degradation by catalytic ozonation based on nickel oxide: study of the ethanol as

cosolvent," *Environmental Science and Pollution Research*, vol. 24, pp. 25550-25560, 2017.

[13] C. Lin, L. Gan, and Z.-L. Chen, "Biodegradation of naphthalene by strain Bacillus fusiformis (BFN)," *Journal of hazardous materials*, vol. 182, pp. 771-777, 2010.

[14] M. Alshabib, "Removal of naphthalene from wastewaters by adsorption: a review of recent studies," *International Journal of Environmental Science and Technology*, vol. 19, pp. 4555-4586, 2022.

[15] B. S. Rathi and P. S. Kumar, "Application of adsorption process for effective removal of emerging contaminants from water and wastewater," *Environmental Pollution*, vol. 280, p. 116995, 2021.

[16] A. Mohammad-Khah and R. Ansari, "Activated charcoal: preparation, characterization and applications: a review article," *Int J Chem Tech Res*, vol. 1, pp. 859-864, 2009.

[17] N. Soltani, A. Bahrami, M. Pech-Canul, and L. González, "Review on the physicochemical treatments of rice husk for production of advanced materials," *Chemical engineering journal*, vol. 264, pp. 899-935, 2015.

[18] M. K. Islam, M. S. Khatun, M. A. Arefin, M. R. Islam, and M. Hassan, "Waste to energy: An experimental study of utilizing the agricultural residue, MSW, and e-waste available in Bangladesh for pyrolysis conversion," *Heliyon*, vol. 7, p. e08530, 2021.

[19] M. Seitzhanova, Z. Mansurov, M. Yeleuov, V. Roviello, and R. Di Capua, "The characteristics of graphene obtained from rice husk and graphite," *Eurasian Chemico-Technological Journal*, vol. 21, pp. 149-156, 2019.

[20] M. S. Ismail, N. Yusof, M. Z. M. Yusop, A. F. Ismail, J. Jaafar, F. Aziz, *et al.*, "Synthesis and characterization of graphene derived from rice husks," *Malays. J. Fundam. Appl. Sci*, vol. 15, pp. 516-521, 2019.

[21] T. Adinaveen, L. John Kennedy, J. Judith Vijaya, and G. Sekaran, "Surface and porous characterization of activated carbon prepared from pyrolysis of biomass (rice straw) by two-stage procedure and its applications in supercapacitor electrodes," *Journal of Material Cycles and Waste Management*, vol. 17, pp. 736-747, 2015.

[22] F. Shahin, "Removal of heavy metals and hormones from wastewater using rice husk and rice straw biochar packed columns," University of Guelph, 2017.

[23] W. S. Hummers Jr and R. E. Offeman, "Preparation of graphitic oxide," *Journal of the american chemical society*, vol. 80, pp. 1339-1339, 1958.

[24] A. Kumar, B. Sengupta, D. Dasgupta, T. Mandal, and S. Datta, "Recovery of value added products from rice husk ash to explore an economic way for recycle and reuse of agricultural waste," *Reviews in Environmental Science and Bio/Technology*, vol. 15, pp. 47-65, 2016.

[25] M. Ahmaruzzaman and V. K. Gupta, "Rice husk and its ash as low-cost adsorbents in water and wastewater treatment," *Industrial & Engineering Chemistry Research*, vol. 50, pp. 13589-13613, 2011.

[26] C. Moliner, D. Bove, and E. Arato, "Co-incineration of rice straw-wood pellets: a sustainable strategy for the valorisation of rice waste," *Energies*, vol. 13, p. 5750, 2020.

[27] S. Brunauer, P. H. Emmett, and E. Teller, "Adsorption of gases in multimolecular layers," *Journal of the American chemical society*, vol. 60, pp. 309-319, 1938.

[28] G. Supriyanto, N. K. Rukman, A. K. Nisa, M. Jannatin, B. Piere, A. Abdullah, *et al.*, "Graphene oxide from Indonesian biomass: Synthesis and characterization," *BioResources*, vol. 13, pp. 4832-4840, 2018.

[29] X. Díez-Betriu, S. Álvarez-García, C. Botas, P. Álvarez, J. Sánchez-Marcos, C. Prieto, *et al.*, "Raman spectroscopy for the study of reduction mechanisms and optimization of conductivity in graphene oxide thin films," *Journal of Materials Chemistry C*, vol. 1, pp. 6905-6912, 2013.

[30] N. Kumar, N. Yadav, N. Amarnath, V. Sharma, S. Shukla, A. Srivastava, *et al.*, "Integrative natural medicine inspired graphene nanovehicle-benzoxazine derivatives as potent therapy for cancer," *Molecular and Cellular Biochemistry*, vol. 454, pp. 123-138, 2019.

[31] O. O. Alegbeleye, B. O. Opeolu, and V. A. Jackson, "Polycyclic aromatic hydrocarbons: a critical review of environmental occurrence and bioremediation," *Environmental management*, vol. 60, pp. 758-783, 2017.

[32] Y. E. Dolaksiz, F. Temel, and M. Tabakci, "Adsorption of phenolic compounds onto calix [4] arene-bonded silica gels from aqueous solutions," *Reactive and Functional Polymers*, vol. 126, pp. 27-35, 2018.

[33] I. Langmuir, "The constitution and fundamental properties of solids and liquids. Part I. Solids," *Journal of the American chemical society*, vol. 38, pp. 2221-2295, 1916.

[34] T. M. Albayati and K. Kalash, "Biosorption technique for naphthalene removal from aqueous solution by Chara sp., algae," *Engineering and Technology Journal*, vol. 36, pp. 1008-1015, 2018.

[35] R. Saadi, Z. Saadi, R. Fazaeli, and N. E. Fard, "Monolayer and multilayer adsorption isotherm models for sorption from aqueous media," *Korean Journal of Chemical Engineering*, vol. 32, pp. 787-799, 2015.

[36] S. Şener and A. Özyılmaz, "Adsorption of naphthalene onto sonicated talc from aqueous solutions," *Ultrasonics sonochemistry*, vol. 17, pp. 932-938, 2010.

[37] M. Dubinin, "The equation of the characteristic curve of activated charcoal," in *Dokl. Akad. Nauk. SSSR.*, 1947, pp. 327-329.

[38] M. Polanyi, "The Potential Theory of Adsorption: Authority in science has its uses and its dangers," *Science*, vol. 141, pp. 1010-1013, 1963.

[39] E. Erdem, N. Karapinar, and R. Donat, "The removal of heavy metal cations by natural zeolites," *Journal of colloid and interface science*, vol. 280, pp. 309-314, 2004.

[40] Ş. S. Bayazit, M. Yildiz, Y. S. Aşçi, M. Şahin, M. Bener, S. Eğlence, *et al.*, "Rapid adsorptive removal of naphthalene from water using graphene nanoplatelet/MIL-101 (Cr) nanocomposite," *Journal of Alloys and Compounds*, vol. 701, pp. 740-749, 2017.

[41] M. Erhayem, F. Al-Tohami, R. Mohamed, and K. Ahmida, "Isotherm, kinetic and thermodynamic studies for the sorption of mercury (II) onto activated carbon from Rosmarinus officinalis leaves," *American Journal of Analytical Chemistry*, vol. 6, p. 1, 2015.

[42] T. M. Albayati and K. R. Kalash, "Polycyclic aromatic hydrocarbons adsorption from wastewater using different types of prepared mesoporous materials MCM-41in batch and fixed bed column," *Process Safety and Environmental Protection*, vol. 133, pp. 124-136, 2020.

[43] V. Ţucureanu, A. Matei, and A. M. Avram, "FTIR spectroscopy for carbon family study," *Critical reviews in analytical chemistry*, vol. 46, pp. 502-520, 2016.

[44] B. Kartick and S. Srivastava, "Green synthesis of graphene," *Journal of nanoscience and nanotechnology*, vol. 13, pp. 4320-4324, 2013.

[45] G. Surekha, K. V. Krishnaiah, N. Ravi, and R. P. Suvarna, "FTIR, Raman and XRD analysis of graphene oxide films prepared by modified Hummers method," in *Journal of Physics: Conference Series*, 2020, p. 012012.

[46] C. Manoratne, S. Rosa, and I. Kottegoda, "XRD-HTA, UV visible, FTIR and SEM interpretation of reduced graphene oxide synthesized from high purity vein graphite," *Mater. Sci. Res. India*, vol. 14, pp. 19-30, 2017.

[47] H. Ha and C. J. Ellison, "Polymer/graphene oxide (GO) thermoset composites with GO as a crosslinker," *Korean Journal of Chemical Engineering*, vol. 35, pp. 303-317, 2018.

[48] J. Guerrero-Contreras and F. Caballero-Briones, "Graphene oxide powders with different oxidation degree, prepared by synthesis variations of the Hummers method," *Materials Chemistry and Physics*, vol. 153, pp. 209-220, 2015.

[49] L. Gu, H. Guo, P. Zhou, N. Zhu, D. Zhang, H. Yuan, *et al.*, "Enhanced adsorptive removal of naphthalene intermediates from aqueous solution by introducing reed straw into sewage sludge-based activated carbon," *Environmental Science and Pollution Research*, vol. 21, pp. 2043-2053, 2014.

[50] A. Lateef, R. Nazir, N. Jamil, S. Alam, R. Shah, M. N. Khan, *et al.*, "Synthesis and characterization of environmental friendly corncob biochar based nano-composite–A potential slow release nano-fertilizer for sustainable agriculture," *Environmental Nanotechnology, Monitoring & Management*, vol. 11, p. 100212, 2019.

[51] M. M. Awad, A. I. Abdel-Salam, S. Elfeky, H. S. Rady, A. S. Hassanien, M. B. Mohamed, *et al.*, "Tuning the optical properties of CdSe quantum dot using graphene nanocomposite," *Journal of Optics*, vol. 48, pp. 616-625, 2019.

[52] L. Stobinski, B. Lesiak, A. Malolepszy, M. Mazurkiewicz, B. Mierzwa, J. Zemek, *et al.*, "Graphene oxide and reduced graphene oxide studied by the XRD, TEM and electron spectroscopy methods," *Journal of Electron Spectroscopy and Related Phenomena*, vol. 195, pp. 145-154, 2014.

[53] N. R. Wilson, P. A. Pandey, R. Beanland, R. J. Young, I. A. Kinloch, L. Gong, *et al.*, "Graphene oxide: structural analysis and application as a highly transparent support

for electron microscopy," *ACS nano*, vol. 3, pp. 2547-2556, 2009.

[54] M. A. Hassan, A. M. Mohammad, T. A. Salaheldin, and B. E. El-Anadouli, "A promising hydroxyapatite/graphene hybrid nanocomposite for methylene blue dye's removal in wastewater treatment," *Int J Electrochem Sci*, vol. 13, pp. 8222-8240, 2018.

[55] S. Brunauer, L. S. Deming, W. E. Deming, and E. Teller, "On a theory of the van der Waals adsorption of gases," *Journal of the American Chemical society*, vol. 62, pp. 1723-1732, 1940.

[56] J. H. Kim, G. H. Shim, T. T. N. Vo, B. Kweon, K. M. Kim, and H. S. Ahn, "Building with graphene oxide: effect of graphite nature and oxidation methods on the graphene assembly," *RSC advances*, vol. 11, pp. 3645-3654, 2021.

[57] P. Dash, T. Dash, T. K. Rout, A. K. Sahu, S. K. Biswal, and B. K. Mishra, "Preparation of graphene oxide by dry planetary ball milling process from natural graphite," *RSC advances*, vol. 6, pp. 12657-12668, 2016.

[58] J. Wang and B. Chen, "Adsorption and coadsorption of organic pollutants and a heavy metal by graphene oxide and reduced graphene materials," *Chemical Engineering Journal*, vol. 281, pp. 379-388, 2015.

[59] S. Maswanganyi, R. Gusain, N. Kumar, E. Fosso-Kankeu, F. B. Waanders, and S. S. Ray, "Bismuth molybdate nanoplates supported on reduced graphene oxide: an effective nanocomposite for the removal of naphthalene via adsorption–photodegradation," *ACS omega*, vol. 6, pp. 16783-16794, 2021.

[60] P. Das, S. Goswami, and S. Maity, "Removal of naphthalene present in synthetic waste water using novel G/GO nano sheet synthesized from rice straw: comparative analysis, isotherm and kinetics," *Front. Nanosci Nanotech*, vol. 2, pp. 38-42, 2016.

[61] A. Kumar and H. Gupta, "Activated carbon from sawdust for naphthalene removal from contaminated water," *Environmental Technology & Innovation*, vol. 20, p. 101080, 2020.

[62] Z. Pei, L. Li, L. Sun, S. Zhang, X.-q. Shan, S. Yang, *et al.*, "Adsorption characteristics of 1, 2, 4-trichlorobenzene, 2, 4, 6-trichlorophenol, 2-naphthol and naphthalene on graphene and graphene oxide," *Carbon*, vol. 51, pp. 156-163, 2013.

[63] S. Yakout, A. Daifullah, and S. El-Reefy, "Adsorption of naphthalene, phenanthrene and pyrene from aqueous solution using low-cost activated carbon derived from agricultural wastes," *Adsorption Science & Technology*, vol. 31, pp. 293-302, 2013.

[64] J. Wang, Z. Chen, and B. Chen, "Adsorption of polycyclic aromatic hydrocarbons by graphene and graphene oxide nanosheets," *Environmental science & technology*, vol. 48, pp. 4817-4825, 2014.

[65] P. Das, S. Goswami, and S. Maiti, "Removal of naphthalene present in synthetic waste water using novel Graphene/Graphene Oxide nano sheet synthesized from rice straw: comparative analysis, isotherm and kinetics," *Frontiers in Nanoscience and Nanotechnology*, vol. 2, p. 38, 2016.

[66] J. Yuan, L. Feng, and J.-X. Wang, "Rapid adsorption of naphthalene from aqueous solution by naphthylmethyl derived porous carbon materials," *Journal of Molecular Liquids*, vol. 304, p. 112768, 2020.

[67] H. Yan, X. Tao, Z. Yang, K. Li, H. Yang, A. Li, *et al.*, "Effects of the oxidation degree of graphene oxide on the adsorption of methylene blue," *Journal of hazardous materials*, vol. 268, pp. 191-198, 2014.